USGS Award Number GP16AP00023

Kinematic and Dynamic Models of the Southern California Lithosphere: Applications to Estimating Crustal Stresses and Stressing Rates

Elizabeth Hearn, Consulting Geophysicist
21 Valley Oak Street, Portola Valley CA 94028
Phone: (408) 334-8075
Fax: 650-329-5163
Email: hearn.liz@gmail.com

Grant Time Period: January 1, 2016 - December 31, 2016

Abstract

Several suites of kinematic models of southern California were developed to investigate (1) discrepancies between geodetic and geologic fault slip rates, (2) stressing rates and (3) how much of the deformation is not due to elastic locking of known, major faults. These models incorporate the UCERF3 block-bounding fault geometry and slip rates from the UCERF3 report (Field et al., 2013). Fault slip rates were randomly sampled from ranges given in the UCERF3 report, and models were scored by their misfit to GPS site velocities and total strain energy (TSE).

All of the model suites (i.e., GPS and TSE constrained models, with or without locking) suggest slip rates of less than about 7 mm/yr on the Ventura-Oak Ridge fault system, consistent with the estimate of Hubbard et al. (2014). Low slip rates (<30 mm/yr) are also strongly preferred for the Mojave section of the San Andreas Fault (SAF). GPS-constrained, locked models suggest high slip rates for the Imperial and Coachella-SAF Faults (40-50 mm/yr and 30-40 mm/yr), with preferred ranges above the UCERF3 maximum values. GPS data also suggest very low slip rates for the San Gorgonio Pass SAF segment (2-7 mm/yr, when the Coachella and Imperial fault slip rates are fixed at their maximum UCERF3 values). Unlocked TSE-constrained models suggest slip rates lower than 40 and 14 mm/yr for the Imperial and Coachella faults. This discrepancy is explained only in part by models with smaller locking depths (representing shallow fault creep on these faults). Low San Gorgonio Pass SAF slip rates are consistent with strain transfer from the SAF Coachella segment to the eastern California shear zone, bypassing the San Gorgonio SAF segment (e.g., Wallace, 1984, Thatcher et al., 2016).

Correcting the SCEC CMM4 GPS velocity field for seismic cycle effects associated with large earthquakes on the 1857 SAF rupture segment increases the inferred slip rate of the Mojave segment of the San Andreas fault by up to about 4 mm/yr, but does not appear to affect inferred slip rates on other segments. Off-fault deformation accounts for 23-32% of the total strain energy accumulation in southern California, depending on how it is calculated. This is consistent with previous estimates (e.g. Field et al., 2013, Johnson, 2013).

Preliminary dynamic models highlight the importance of upper crustal plasticity on inferred stress amplitudes, stress axis orientations and fault slip rates in southern California.

1. Introduction

This report is for a follow-on proposal, which together with our 2015 proposal describes a research program addressing the kinematics and dynamics of southern California faults. For the kinematic modeling part of this work, I developed suites of finite-element models to assess fault slip rates, seismic-cycle effects on slip rates inferred from surface deformation, and the proportion of current deformation that is not explained by the model ("off fault deformation"). For the dynamics part, I investigated the importance of fault zone tractions (a proxy for rheology) and crustal plasticity on inferred crustal stresses and fault slip rates. This report will focus primarily on the kinematic model results, which are being readied for publication.

Kinematic modeling based on the finite-element approach differs substantially from block modeling that has been done in southern California in the past because strains may vary in a complicated fashion within fault-bounded blocks. In terms of relating "off-fault" moment accumulation to geodetic-geologic slip rate discrepancies, the approach I describe above is analogous to that taken by Marshall et al. (2013) with boundary element models covering a smaller region within southern California. In terms of relating viscoelastic earthquake-cycle effects ("ghost transients") to geodetic-geologic slip rate discrepancies, this approach is analogous to that of Pollitz et al. (2008), Chuang and Johnson (2011), Johnson (2013), and Hearn et al. (2013). The power of using finite elements for this problem is that both effects have been taken into account with the same model.

In my 2015 proposal, the specific tasks related to kinematic modeling were:

- *Find the minimum strain energy solution (for the unlocked case and the locked case)*
- *Compute minimum GPS misfit solutions (for the unlocked case and the locked case)*
- Compute ghost transients at all GPS sites for a small suite of large earthquakes and Earth models.
- Interpret the results to place constraints on off-fault deformation and GPS-Holocene slip rate discrepancies

A new task for this 2016 continuation proposal was:

- Implement Bayesian/MCMC inversion for slip rates

The tasks in italics were completed prior to the 2016 grant period. The remaining tasks were completed in 2016 and are described in this report. Additional model suites were run in 2016 using the MCMC inversion approach and other strategies to improve slip rate estimates.

2. Methods

I use GAEA, a three-dimensional viscoelastic finite-element code that makes use of isoparametric, quadratic hexahedral (Q2) elements (Saucier and Humphreys, 1993) for the kinematic modeling. GAEA has been benchmarked against semi-analytical and numerical codes for elastic and viscoelastic deformation (e.g., VISCO1D, the Savage and Prescott [1978] seismic cycle solution, the uniform and layered elastic dislocation solutions of Okada [1985] and Wang et al. [2006]; Hearn and Bürgmann, 2005; Hearn and Thatcher, 2015, Hearn, 2003). For elasto-plastic static deformation problems, Q2 elements outperform linear hexahedral and tetrahedral elements and quadratic tetrahedral elements (e.g., Benzley et al., 1995), and the mesh (part of which is shown in Figure 1) represents deformation with a level of precision comparable to a mesh with eight times the number of the more commonly used linear block elements. All elements are elastic with G = 30 GPa and v = 0.25.

2.1 Mesh and Boundary Conditions

The finite element (FE) model mesh representing the southern California lithosphere is unstructured, allowing better resolution in areas of geometric complexity. The mesh currently comprises 18840 nodes and 3651 elements (equivalent to about 32,000 linear block elements), and covers a region of 1200 x 1600 km. For the kinematic models, the mesh is 80 km deep and is rotated 35 degrees to align its left and right boundaries with the Pacific-North America plate boundary.

Deformation occurs in response to imposed velocity boundary conditions at the sides of the model (constrained by GPS), and by imposed slip on those fault segments that are represented with split nodes (see below). Elements along the left model boundary move at the Pacific-North America relative rate, with a slight counter-clockwise rotation (De Mets et al., 2010). The right side moves west-northwest relative to North America at rates of 1-2 mm/yr, as interpolated from the SCEC CMM4 GPS velocity field (Shen et al., 2011). The north, south and top boundaries are traction-free, and the bottom boundary is free to displace horizontally.

2.2 Faults

Major faults represented in my model coincide with block boundaries from the UCERF3 block models, which are in turn defined by major fault traces from the UCERF3.1 fault model (Field et al., 2013, Appendix B and Table B1). Figure 1 shows part of the finite-element mesh with several of the 50 modeled fault segments highlighted. Table 1 shows model-pertinent information associated with each of these segments. A model fault bisecting the Transverse Ranges (the ‘Ventura-Oak Ridge Fault’), is not part of the UCERF3.1 block model but has been added to account for shortening across the San Cayetano, Ventura, Oak Ridge, Red Mountain and other faults in this region. Two low-rate block-bounding faults have been excluded (White Wolf and Great Valley faults). In the Mojave region, the Landers-Gravel Hill and Pisgah-Blackwater faults have been collapsed to a single structure.

The major faults are represented using split nodes (with specified offsets and slip vectors, Melosh and Raefsky, 1981), slippery nodes (with slip rates that minimize shear stresses along the fault surface, Melosh and Williams, 1989) or "free" nodes, in with the model solves for both the magnitude and orientation of the slip vector. Blind thrust faults of the Los Angeles Basin are not represented in the model, though this area likely accommodates several mm per year of NNE-SSW shortening (per discussions with Tim Dawson and Kate Scharer in May 2015, also the 2015 SSA Annual Meeting field trip guide). Fault slip rates are randomly sampled from intervals provided in the UCERF3 report (Field et al., 2013). Table 1 summarizes slip rate ranges for faults represented in this study.

2.3 Inversions for Slip Rates

Fault slip rates are randomly drawn from ranges on Table 1, and the model is run 10,000 times. For each run, the weighted residual sum of squares (WRSS) misfit to GPS velocities, and the total strain energy are computed and stored. Though the model domain extends far beyond southern California, only velocities and strain energies from model elements in southern California are counted in the inversion.

The "classic" Monte Carlo inversion involves running 10,000 models and calculating the weighted residual sum of squares (WRSS) misfit to GPS velocities and total strain energy (TSE) for each. For each of the 10,000 models, fault slip rates are randomly sampled from UCERF3 ranges (Field et al., 2013) assuming boxcar or normal distributions. Slip vector orientations are not varied.

When the unscaled CMM4 formal error ranges are assumed, weighted residual sum of squares (WRSS) misfits to the GPS velocities are large. Like Johnson (2013), I chose to scale up the formal velocity uncertainties to generate a normalized weighted residual quantity with a minimum value of about 1. One-sigma formal velocity errors (i.e. 68% confidence intervals) were scaled by a factor of five, and any values that were still below 0.5 mm/yr (after scaling) were set to 0.5 mm/yr. Data from three GPS sites where velocity vectors did not resemble others in the area were effectively removed from the inversion by setting their formal errors to large values. GPS sites in the vicinity of the Hector Mine, Landers and El Mayor earthquakes were not removed, nor were they corrected for postseismic effects.

Total strain enemy is computed as the product of the stress and strain tensors at the center of each model element, times the element volume. The computation is restricted to the shallowest elements. Strain energy is scaled to obtain a value of 1 for the minimum TSE model from suite 2A.

In addition to the Monte Carlo inversion method described above, I implemented two Markov Chain Monte Carlo (MCMC) methods: Independence Sampler MCMC and Random Walk Metropolis-Hastings MCMC. The Independence Sampler method involves random sampling of slip rates (within a boxcar range or a truncated normal distribution) but after each case is run, the solution is either accepted or rejected based on how well it fits the GPS velocities (or how low

the model strain energy is) compared to the previous solution. Models that better fit the constraints (i.e., have a higher likelihood value) are more likely to be accepted than models that perform more poorly. The next sample of slip rates is randomly drawn from the same distribution as before, regardless of whether the model was accepted or not. The random walk Metropolis-Hastings method takes into account previous guesses by sampling parameters from distributions around values from the most recent accepted model, rather than from pre-ordained distributions. In both cases, the solution becomes insensitive to the initial set of assumed slip rates after a burn-in period, and accepted models should define a probability distribution of slip rates for individual fault segments.

Inferred slip rates appear to be independent of the inversion technique I use - that is, MCMC inversions and least-squares Monte Carlo inversions point to the same preferred slip rate ranges. However, neither of the MCMC methods resolves slip rates as well as the least-squares Monte Carlo approach. I show results for both techniques. To estimate slip rate errors, I use the approach described by Johnson (2013, Figure 16), though this approach may be overly conservative.

2.4 Model Suites

Several suites of 10,000 kinematic models were run, with locked or unlocked faults, and calibrated to the SCEC CMM4 GPS velocity field, a version of this velocity field corrected for viscoelastic earthquake cycle effects, or a total strain energy (TSE) minimization constraint. Suite 1 comprises locked models calibrated to the SCEC CMM4 velocity field. Suite 2 comprises unlocked models calibrated to a strain energy minimization constraint. An additional suite of locked models (Suite 1A) is calibrated to a version of the GPS velocity field that has been corrected for viscoelastic seismic cycle effects due to large quakes on the 1857 rupture segment. The correction was calculated using VISCO1D (Pollitz, 1997) with earthquake and elasticity parameters from Hearn et al. (2013). The modeled earthquakes extend through a 25 km thick elastic upper plate. Below this an effective viscosity of 5×10^{19} Pa s is assumed down to a depth of 270 km, where it increases by a factor of ten.

Additional model suites (Table 2) assume restricted slip rate ranges for faults where a clear preference was shown in Model Suite 1 or 2. A strain energy minimizing model suite incorporating locked faults (Suite 2A) was run to estimate interseismic strain energy contribution due to the modeled faults, which is required to isolate “off-fault” strain accumulation.

3 Results and Conclusions

The kinematic models yield clear slip rate preferences for some (though not most) fault segments (Tables 3A and 3B). The largest surface velocity residuals are evident in the areas of the Landers, Hector Mine and El Mayor-Cucapah earthquakes (Figure 2). Typical residuals for the best Suite 1A-D models are of the order of 1-3 mm/yr.

The largest differences between modeled slip rates and UCERF3 geologic slip rates are for the Ventura-Oak Ridge system and the Mojave segments of the SAF. Both GPS- and TSE-constrained models suggest lower rates for these faults. Modeled slip rates for the San Gorgonio Pass section of the SAF also fall toward the bottom of the UCERF3 range, particularly for GPS-constrained models. The largest differences in estimated slip rate between TSE- and GPS-constrained models are for the Coachella, Imperial and northern San Jacinto faults.

Figure 3 shows model sensitivity to slip rates on the S Mojave SAF, based on how well models fit GPS data or minimize strain energy. Similar plots were made for all of the modeled fault segments, and fault slip ranges were estimated by fitting the minimum TSE or WRSS values for each slip rate (or values for accepted MCMC models at that slip rate) to a quadratic function of slip rate. Admissible slip rate ranges reported on Tables 3A and 3B are those for which at least one model produced a TSE or WRSS misfit within 2% of the best value for the suite (after Johnson, 2013).

Southern San Andreas Fault system. Within the UCERF3 slip rate ranges, the GPS-constrained Suite 1 models prefer low slip rates on the Mojave segments of the SAF (< 25 mm/yr); and high rates on the northern section of the San Jacinto Fault, the Imperial Fault and the Coachella segment of the San Andreas fault (>13 mm/yr, >38 mm/yr and >30 mm/yr). Suite 2 models suggest low slip rates on the Coachella and north San Jacinto faults (<14 mm/yr and <11 mm/yr). Reducing locking depths on the Coachella, Imperial and central San Jacinto segments allows some overlap between admissible slip rate ranges for GPS- and strain energy-constrained models. However, further refinement of the model and efforts to reconcile these slip rates should take into account a possible active fault strand about 10 km west of the Imperial Fault (Lindsey and Fialko, 2016).

Transverse Ranges. All of the models prefer a rate of convergence at the low end of the UCERF3 range for the Ventura-Oak Ridge fault system within the Transverse Ranges (i.e. 3 to 10 mm/yr; Figure 1). Slip rate ranges for the Ventura-Oak Ridge fault system estimated from the UCERF3 report are 1.5 to 15 mm/yr (summing rates for the Ventura/Pitas Point and Red Moun- tain faults) and 3.2 to 15 mm/yr (summing rates for the Oak Ridge and San Cayetano faults). My inferred slip rate (< 7 mm/yr) is consistent with the recent estimate from Hubbard et al. (2014) of 4.4 to 6.9 mm/yr. Though both the minimum TSE and GPS misfit constraints indicate a low slip rate, the GPS constraint is much stronger.

Effect of viscoelastic perturbation to the GPS velocity field. Correcting the GPS velocity field for seismic cycle effects associated with the 1857 rupture segment of the SAF has a modest yet significant effect on slip rates inferred for the Mojave segment of the SAF (Figure 4). A higher slip rate (by about 4 mm/yr) is preferred for the Mojave segment of the SAF, though for other fault segments the effect of the correction is negligible. Given that the viscoelastic correction assumed a thin lithosphere and a modest (5×10^{19} Pa s) substrate viscosity, the GPS velocity perturbation we have calculated is an upper limit. This suggests that viscoelastic perturbations to

the surface deformation field have only a limited influence on individual fault slip rates in our model.

Off-fault deformation. Contributions to present-day surface deformation arise from (1) inter-seismic, elastic locking of modeled faults, (2) steadily accumulating "off-fault" deformation, and (3) viscoelastic earthquake-cycle and human-induced effects. As noted above, I have computed (3) using a viscoelastic seismic cycle model and used this to adjust the SCEC CMM4 velocity field. One suite of locked models (Suite 1A) is calibrated to this field. An unlocked model suite set to minimize strain energy (Suite 2) should provide an estimate of off-fault deformation, and the best models in Suites 1A and 2 should have identical slip rates. A comparison of strain energy values in the upper crust for these two models provides the best self-consistent estimate of the proportion of strain energy that is not associated with locking of known, major faults. If seismic cycle effects are negligible, then a comparison of the best Suite 1 and Suite 2a models (presumably, with identical slip rates) should provide an accurate estimate of the off-fault strain energy budget in the upper crust.

I selected slip rate ranges for major faults in Suite 2 that were within the UCERF3 ranges, and for which at least one model had a minimum strain energy of less than 6.6×10^{18} J/y (counting model elements in southern California and adjoining areas). I refined the admissible slip rate ranges by finding Suite 1 models with slip rates in these ranges and a minimum normalized WRSS of less than 1.2. Strain energies from Suite 1 and Suite 2 models incorporating slip rates within the admissible ranges for both suites were compared. Using 11 MCMC-accepted Suite 1 models and 19 accepted Suite 2a models, I estimated mean strain energies (and standard deviations) of $3.70 (\pm 0.30) \times 10^{19}$ N m/y and $8.67 (\pm 1.20) \times 10^{18}$ N m/y respectively, and a ratio of 0.23 (±0.04), meaning that about a quarter of the apparently accumulating strain energy is off-fault deformation. Doing the same exercise but with Suite 1A models, I obtain 0.24 (±0.04). If I simply compare the best Suite 1 model (with normalized WRSS = 1.0 and strain energy = 2.0×10^{19} N m/y) with the best Suite 2 model (with strain energy = 6.0×10^{18} N m/y and normalized WRSS = 2.7), without requiring that they have consistent slip rates, I estimate that 32% of the strain energy is from off- fault deformation. Both estimates are consistent with other recent studies (e.g. Zeng and Shen, 2016).

Effect of refining GPS-constrained models. Model suites were run holding slip rates for the Imperial and Coachella faults constant at the best GPS-inferred rates (40 and 30 mm/yr, respectively, identical to the maximum UCERF3 rates), both with and without the SAF ghost transient correction (Suites 1B and 1C). This reduced the inferred San Gorgonio Fault slip rate from 2.5-12 mm/yr to 2.5-7.3 mm/yr, for both suites. These slip rates overlap with UCERF3 range for the San Gorgonio Pass SAF (4-7.3 mm/yr). Setting the Imperial and Coachella slip rates to their maximum UCERF3 values also limits the GPS-constrained Mojave SAF slip rate to less than 23 mm/yr.

Slip rates from dynamic models. Several elastic and elasto-plastic versions of the southern California model have been run, with varied shear tractions along the San Andreas and other faults. Where plasticity is assumed, computations require iteration and take many hours to run, so my explorations have consisted of comparing the results of judiciously selected forward models. Figure 5 shows how plasticity affects slip rates for models in which the SAF is modeled as traction-free fault. When plasticity is assumed (using Drucker-Prager parameters from Liu et al., 2010), the modeled SAF slip rate is significantly higher (35-40 mm/yr in southern CA) and slip is less variable along the fault. (This finding is borne out by test models with a straight strike-slip fault hosting an extensional stepover.) Adding the San Jacinto and Garlock faults as traction-free surfaces reduces the SAF slip rate in the San Gorgonio Pass region and to the south, and the San Jacinto rate exceeds that of the SAF immediately to its east. Quantitative comparison of dynamically modeled fault slip rates to geologic and kinematically modeled rates will begin after all of the faults are added to the model, and will continue as basal tractions, rheological heterogeneities, and gravitational body forces are added to the model.

References

Benzley, S. E., E. Perry, K. Merkley, B. Clark, and G. Sjaardama (1995), A comparison of all hexagonal and all tetrahedral finite element meshes for elastic and elasto-plastic analysis, In *Proceedings, 4th International Meshing Roundtable*, vol. 17, pp. 179-191, Sandia National Laboratories Albuquerque, NM.

Chuang, R. Y. and K. M. Johnson (2011), Reconciling geologic and geodetic model fault slip-rate discrepancies in Southern California: Consideration of nonsteady mantle flow and lower crustal fault creep, *Geology*, 39(7), 627-630.

De Mets, C., R. G. Gordon and D. F. Argus (2010), Geologically current plate motions, *Geophys. J. Int.*, 181(1), 1-80.

Field, E.H. et al. (2013), Uniform California earthquake rupture forecast, version 3 (UCERF3)—The time-independent model: *U.S. Geological Survey Open-File Report 2013–1165*, 97 p., California Geological Survey Special Report 228, http://pubs.usgs.gov/of/2013/1165/.

Hearn, E. H. and R. Bürgmann (2005). The effect of elastic layering on inversions of GPS data for coseismic slip and resulting stress changes: Strike-slip earthquakes, *Bull. Seis. Soc. Am.*, 95(5), 1637-1653.

Hearn E. H., F. F. Pollitz, W. R. Thatcher, and C. T. Onishi (2013), How do "ghost transients" from past earthquakes affect GPS slip rate estimates on southern California faults?, *Geochem. Geophys. Geosyst.*, 14, 828–838, doi:10.1002/ggge.20080.

Hubbard, J. et al. (2014), Structure and seismic hazard of the Ventura Avenue anticline and Ventura fault, California: Prospect for large, multisegment ruptures in the Western Transverse Ranges, *Bull. Seis. Soc. Am.*, 104, 1070-1087.

Johnson, K. M. (2013), Slip rates and off-fault deformation in Southern California inferred from GPS data and models, *J. Geophys. Res.*, 118, doi:10.1002/jgrb.50365.

Lindsey, E. O. and Y. Fialko (2016), Geodetic constraints on frictional properties and earthquake hazard in the Imperial Valley, Southern California, *J. Geophys. Res.,* 121(2), 1097-1113.

Liu, M., H. Wang, and Q. Li (2010), Inception of the eastern California shear zone and evolution of the Pacific−North American plate boundary: From kinematics to geodynamics, *J. Geophys. Res.,* 115, B07401.

Marshall, S.T., G. J. Funning, and S. E. Owen (2013), Fault slip rates and interseismic deformation in the western Transverse Ranges, California, *J. Geophys. Res.,* 118.8, 4511-4534.

Melosh, H. J. and A. Raefsky (1981). A simple and efficient method for introducing faults into finite element computations, *Bull. Seis. Soc. Am.*, 71(5), 1391-1400.

Melosh, H. J. and C. A. Williams (1989), Mechanics of graben formation in crustal rocks: A finite element analysis. *J. Geophys. Res.*, 94, 13961-13973.

Okada, Y., Surface deformation due to shear and tensile faults in a half-space, *Bull. Seis. Soc. Am.,* 75.4, 1135-1154.

Pollitz, F.F., 1997. Gravitational viscoelastic postseismic relaxation on a layered spherical Earth. *J. Geophys. Res., 102*(B8), 17921-17941.

Pollitz, F. F. (2008), Observations and interpretation of fundamental mode Rayleigh wavefields recorded by the Transportable Array (USArray), *J. Geophys. Res.*, 113, B10311, doi: 10.1029/2007JB005556.

Saucier, F. and E. D. Humphreys (1993), Horizontal crustal deformation in Southern California from joint models of geologic and very long baseline interferometry measurements, *Contributions of Space Geodesy to Geodynamics: Crustal Dynamics*, 139-176.

Shen, Z. K., R. W. King, D. C. Agnew, M. Wang, T. A. Herring, D. Dong and P. Fang (2011). A unified analysis of crustal motion in Southern California, 1970–2004: The SCEC crustal motion map, *J. Geophys. Res.*, 116, B11402, doi:10.1029/2011JB008549.

Thatcher, W., J. C. Savage, and R. W. Simpson (2016), The Eastern California Shear Zone as the northward extension of the southern San Andreas Fault, *J. Geophys. Res.*, 121, 2904–2914, doi:10.1002/2015JB012678.

Traoré, N. et al. (2014), Does interseismic strain localization near strike-slip faults result from boundary conditions or rheological structure?, *Geophys. J. Int.*, 197(1), 50-62.

Wallace, R. E. (1984), Patterns and timing of late Quaternary faulting in the Great Basin province and relation to some regional tectonic features, *J. Geophys. Res.*, 89, 5763-5769.

Yang, W. and E. Hauksson (2013), The tectonic crustal stress field and style of faulting along the Pacific North America Plate boundary in Southern California, *Geophys. J. Int.*, 194(1), 100-117.

Zeng, Y. and Z. K. Shen (2016), A Fault-Based Model for Crustal Deformation, Fault Slip Rates, and Off-Fault Strain Rate in California, *Bull. Seis. Soc. Am.*, 106(2), 766-784.

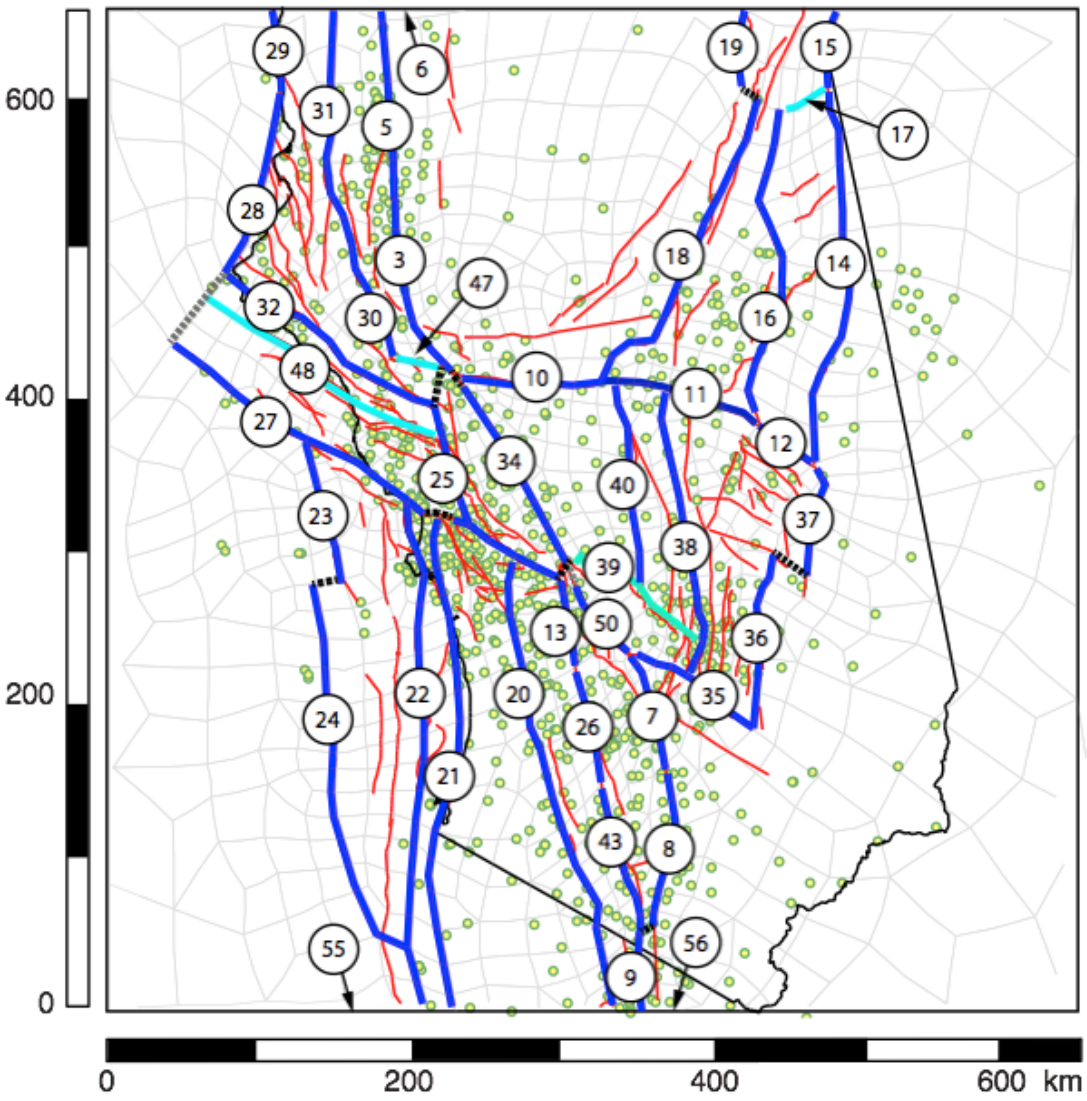

Figure 1. Part of the finite-element mesh covering southern California and the surrounding region (see text for details). Blue, cyan, black dashed and gray dashed lines show modeled strike-slip, dip-slip, free slip and slippery node faults. Red lines are mapped faults and green dots are SCEC CMM4 velocity field GPS stations. Numbers identify fault segments, see Table 1.

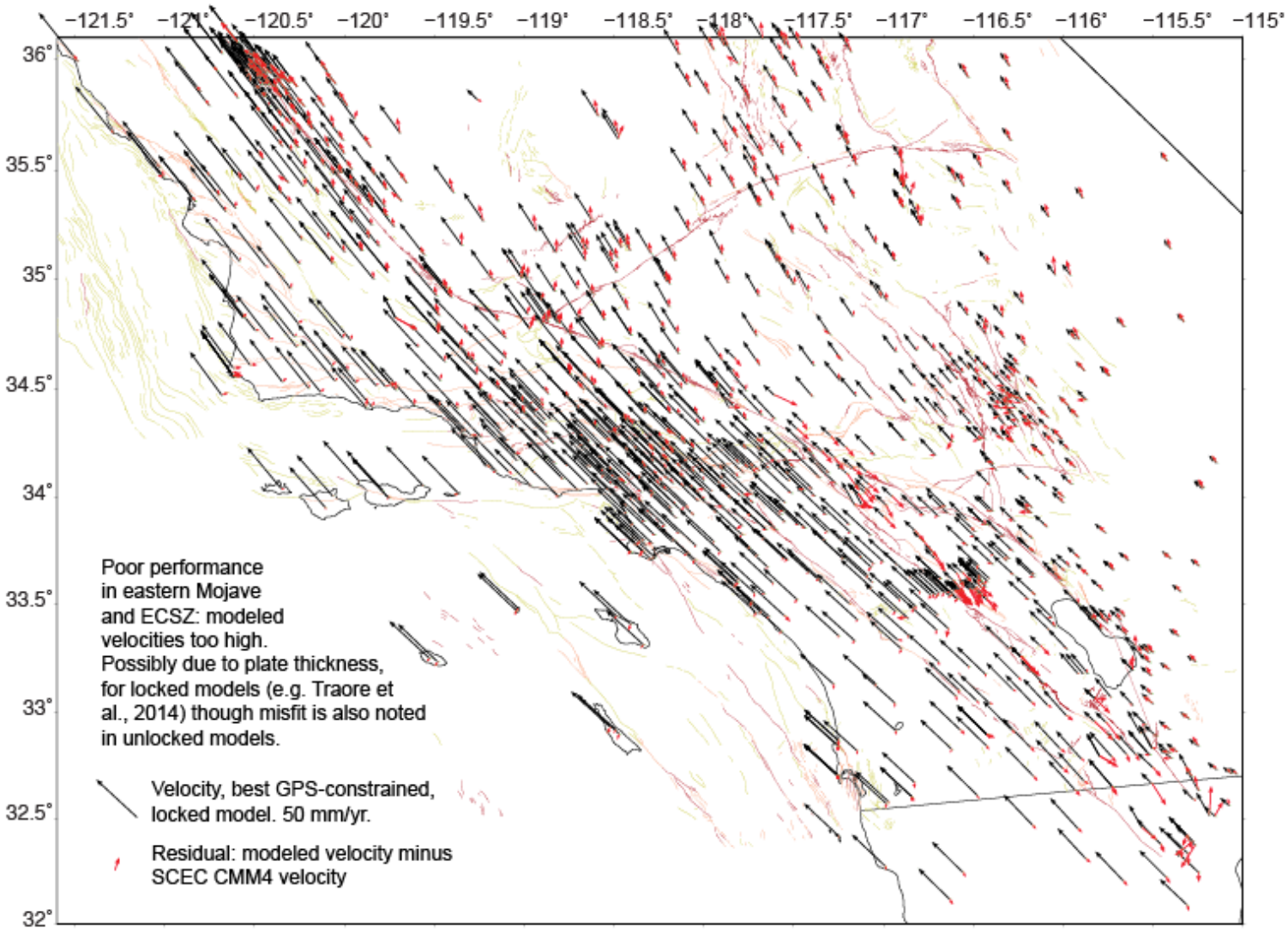

Figure 2. Modeled GPS site velocities and residuals for a model in Suite 1. Significant misfit is visible in the Mojave and the southern California border region, where large earthquakes have affected the GPS velocity field. This particular model sampled too-high slip rates for ECSZ faults, resulting in significant misfit to GPS velocities in that area.

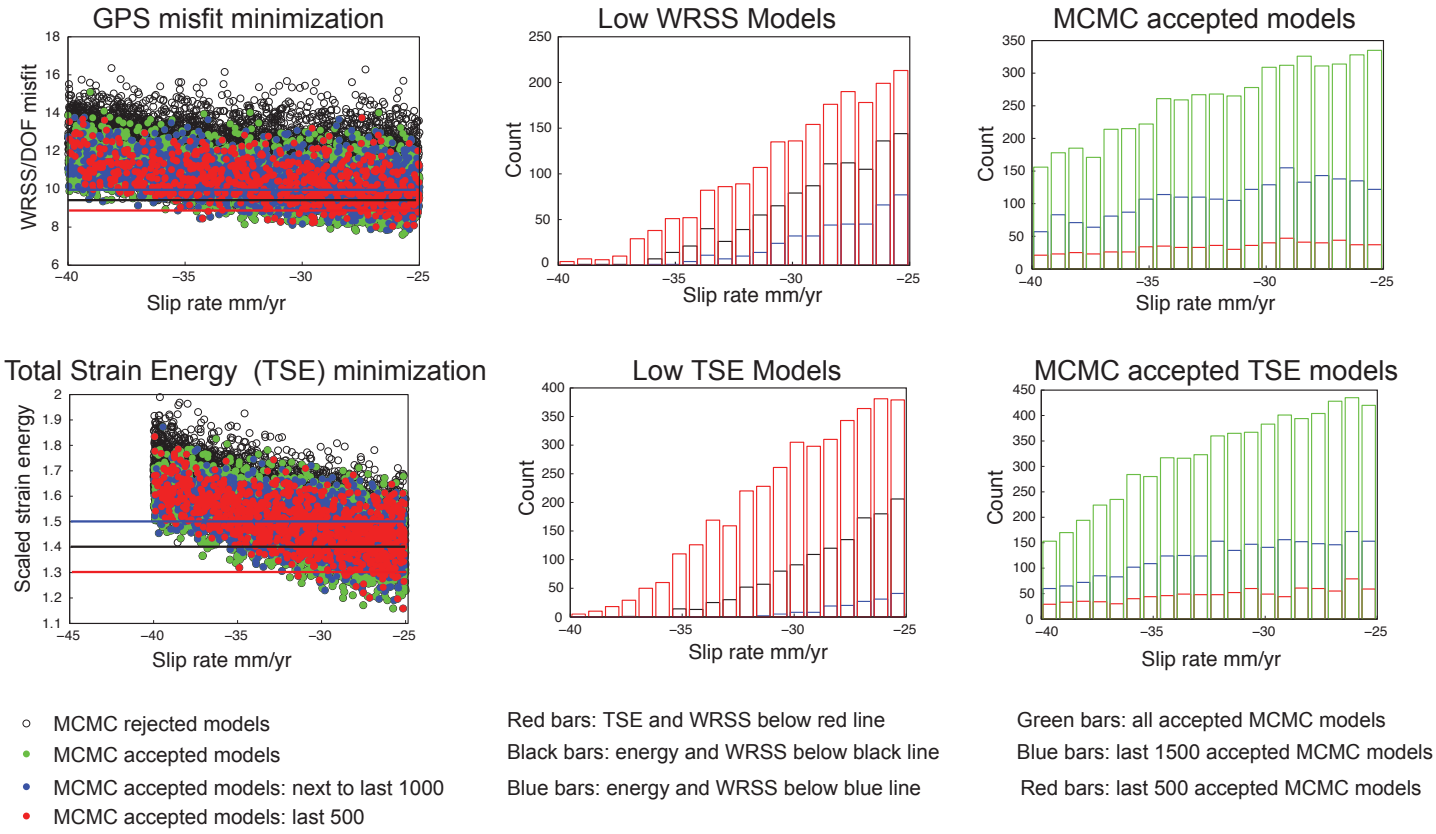

Figure 3. Sensitivity of GPS velocity field misfit and total strain energy (TSE) to variations in the Mojave-SAF slip rate. The two left panels show weighted residual sum of squares (WRSS) misfit to GPS velocities (top) and TSE (bottom) as a function of the slip rate on model segment 34 (Mojave segment of the SAF). Middle panels show histograms of the number of models with WRSS misfit or TSE below thresholds indicated by the red, black and blue lines on the left panels. The best-performing models are likely to have low slip rates (25-30 mm/yr). Right panels show histograms of various indicated populations of accepted Independence Sampler MCMC models. The histograms have been corrected to correct for differences in the number of models run at each slip rate. Bar colors are keyed to dot colors for individual models on the two left panels. Though the accepted MCMC models are more likely to have low slip rates, the preference is not as stark as it is for the center panels.

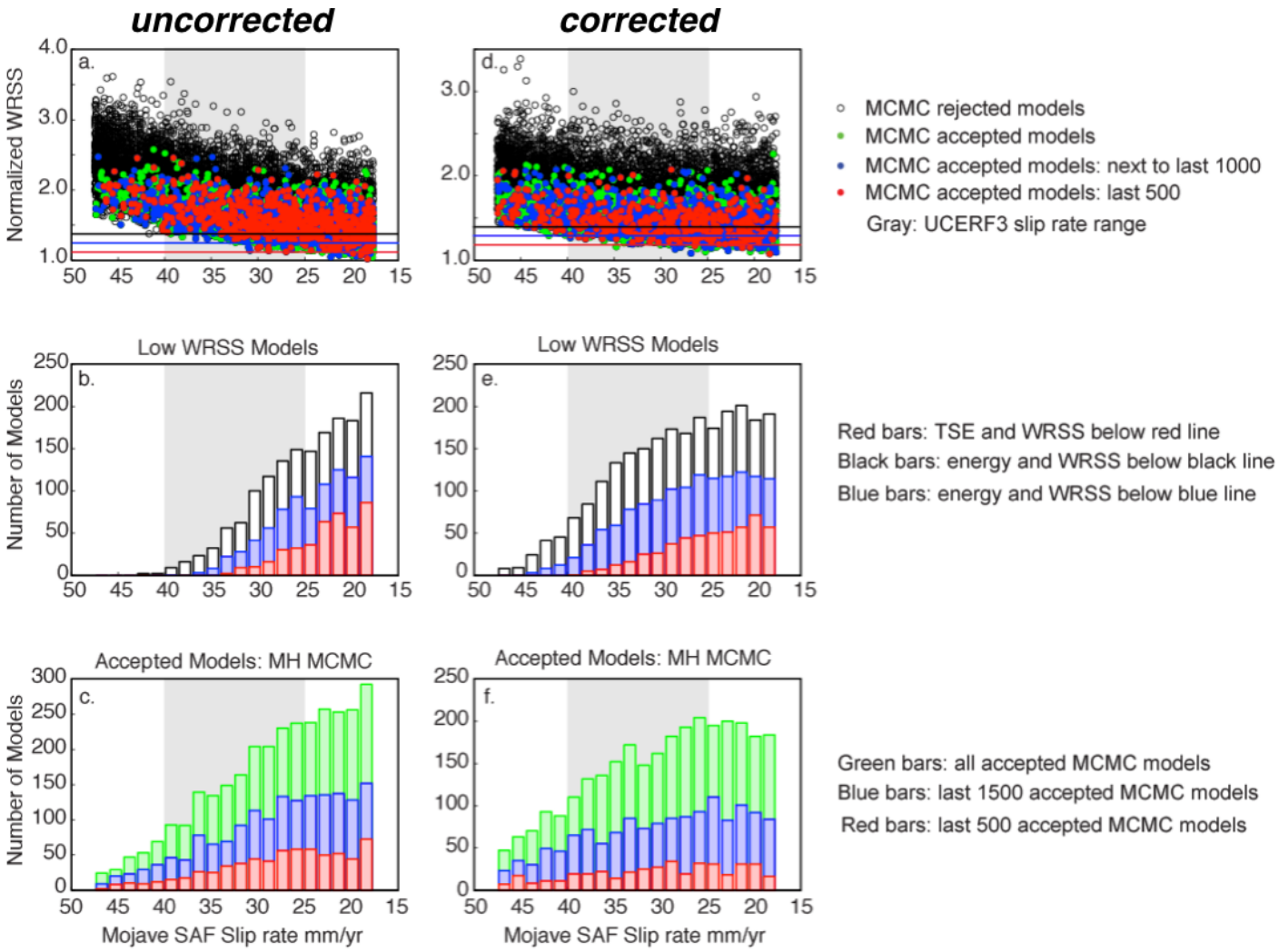

Figure 4. Effect of viscoelastic seismic cycle effects on inferred Mojave slip rates. Top: normalized WRSS versus slip rate for all 10,000 models, for uncorrected (left) and corrected (right) GPS velocity fields. Middle panels: histograms showing number of models with normalized WRSS below thresholds shown on top panels. Bottom: histograms of indicated populations of accepted MCMC models (Random walk method, sampling from Gaussian distributions of slip rates). The histograms have been corrected to correct for differences in the number of models run at each slip rate.

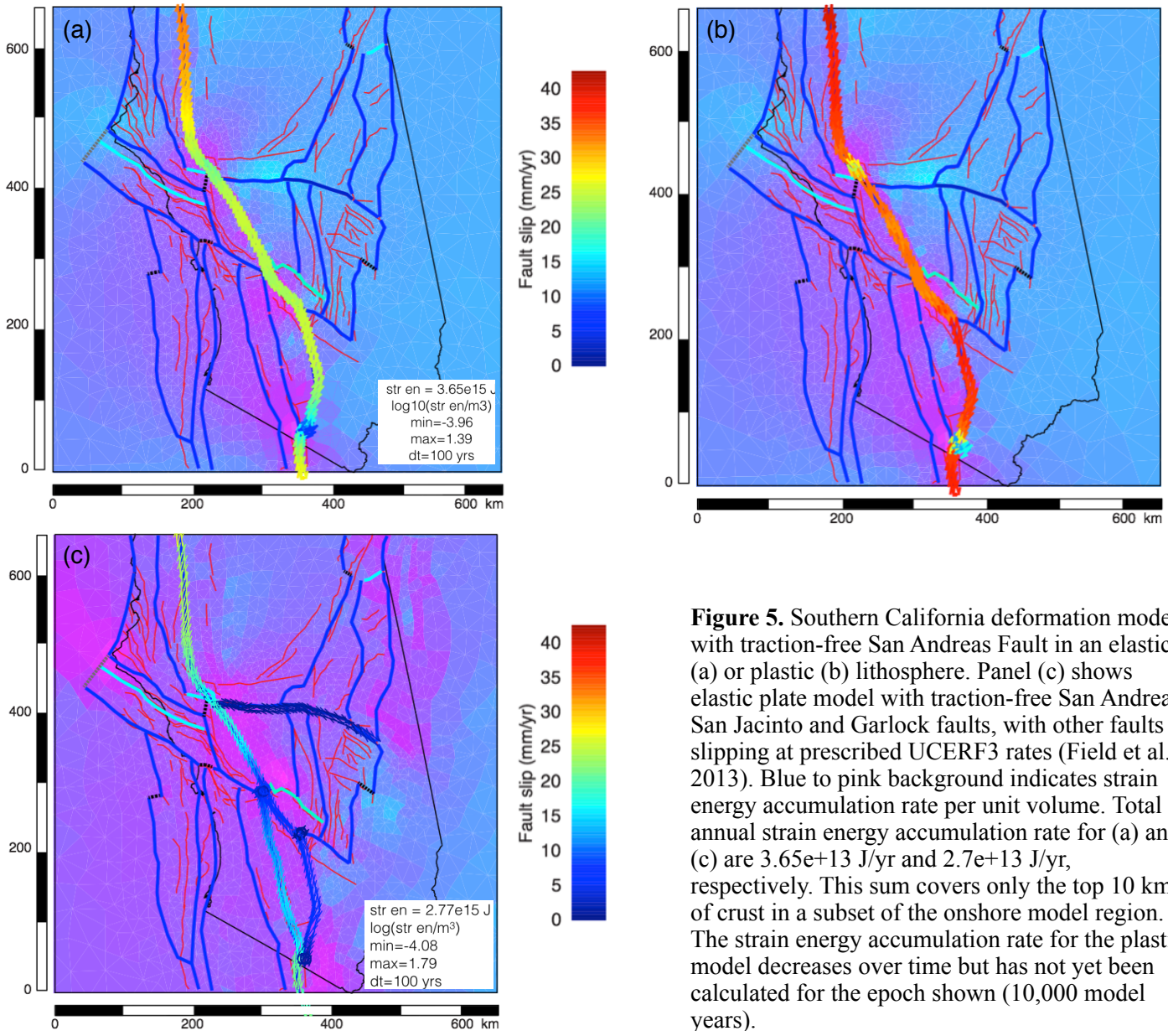

Figure 5. Southern California deformation models with traction-free San Andreas Fault in an elastic (a) or plastic (b) lithosphere. Panel (c) shows elastic plate model with traction-free San Andreas, San Jacinto and Garlock faults, with other faults slipping at prescribed UCERF3 rates (Field et al., 2013). Blue to pink background indicates strain energy accumulation rate per unit volume. Total annual strain energy accumulation rate for (a) and (c) are 3.65e+13 J/yr and 2.7e+13 J/yr, respectively. This sum covers only the top 10 km of crust in a subset of the onshore model region. The strain energy accumulation rate for the plastic model decreases over time but has not yet been calculated for the epoch shown (10,000 model years).

TABLE 1 Fault Node Group Definitions

Group	Name	UCERF3 Avg Rate range	UCERF3 Category	Split or slippery	Slip sense	Notes
3	SAF Mojave N	25-40 (34)	B	split	RL	
4	slippery nodes			slippery	RL or LL	strike slip, model solves for slip. this group is for moderate to high rate segments where slip rate changes over a short distance
5	SAF Carrizo	31-37 (34)	A	split	RL	
6	SAF to north bdry	31-37 (34)		split	RL	use Carrizo rate
7	SAF San Bernardino (S)	5-20 (13)	A	split	RL	
8	SAF Coachella	15-30 (20)	A	split	RL	
9	Imperial	15-40 (35)	C	split	RL	
10	West Garlock	5-11 (6-7.6)	A	split	LL	
11	Central Garlock	5-9 (7)	A	split	LL	
12	East Garlock	1-5 (3)	NA	slippery	LL	
13	San Jacincto (N)	11-18 (14)	B	split	RL	
14	Death Valley	3-6 (4.5)	A	split	RL-normal	“Northern DVF” rate of UCERF3
15	Fish Lake Valley	2-4 (3)	A	split	RL	Not named in UCERF3 report on the map? Corresponds with “N of DVF on KJ’s block model map 6/11
16	Panamint Valley	1-5 (3)	A	split	RL-normal	
17	Deep Springs	0.7-1.7 (1.2)	B	split	normal	
18	S Range Front	0.2 to 0.5 (0.3)	A	split	normal	

Group	Name	UCERF3 Avg Rate range	UCERF3 Category	Split or slippery	Slip sense	Notes
19	Owens Valley (and N Range Front)	2-5 (3.5)	A	split	RL-normal	collapsed onto the same structure, modeled as RL N RFF rate is unknown but UCERF3 assumes 0.2-0.5 (.3)
20	Elsinore	3-7 (5)	A	split	RL	rate drops to 1-5(3) heading S, B. Divide?
21	Newport-Inglewood	0.5-3 (1)	C	split	RL	
22	Palos Verdes	2-5 (3)	A	split	RL	
23	N San Clemente	1.5-5 (1.8)	D	split	RL	use “San Clemente” info rate “appears too high” according to UCERF3
24	S San Clemente	1.5-5 (1.8)	D	split	RL	use “San Clemente” info
25	San Gabriel Fault	0.2-1 (0.39)	C	split	LL	1 mm/yr per SSA field trip
26	North-Central San Jacinto (Anza)	11-18 (14)	A	split	RL	
27	Santa Cruz Islands	0.2-1 (0.9)	A	split	LL/R	oblique, mostly horizontal, rake is 30 degrees, dip is 90
28	S Hosgri	1-5 (2.5)	B	slippery	RL	“Hosgri" rate is given by UCERF3, but UCERF3 states that the rate likely decreases to the S.
29	Central to N Hosgri	1-5 (2.5)	B	split	RL	“Hosgri" rate from UCERF3.
30	Rinconada S	0.2-1 (0.4)	D	split	RL	“Rinconada” rate based on USGS rate category and low geomorphic expression
31	Rinconada N	0.2-1 (0.4)	D	split	RL	“Rinconada” rate based on USGS rate category and low geomorphic expression
32	Santa Ynez	0.2-3 (2)	D	split	LL	
33	Sierra Madre-Cucamonga	1-3 (2)	A	split	R	Important thrust F, 45-53 degree dip USGS : 1-5
34	SAF Mojave S	25-40 (34)	B	split	RL	south of Garlock junction

Group	Name	UCERF3 Avg Rate range	UCERF3 Category	Split or slippery	Slip sense	Notes
35	Pinto Mountain	1-5 (2.5)	D	split	LL	
36	SE Mojave Boundary	na	na	free-splitting	RL-normal?	“ECSZ Eastside” in UCERF3 block model. No Quaternary rates in USGS database.
37	NE Mojave Boundary	na	na	free-splitting	RL-normal?	“ECSZ Eastside” in UCERF3 block model. No Quaternary rates in USGS database.
38	Landers-Gravel Hill	0.5-2.1 (1.1)	NA	split	RL	segment name and geometry per UCERF3 model. Follows Landers, Harper faults. UCERF3 block model has a parallel fault to the E, my model does not, hence rates combine. (Pisgah - Blackwater fault, including Hector Mine rupture). Uncertain combined rate due to Gravel Hills/Harper/ Landers faults (no Quat rates) Combined rate should be about 0.5 to 2.1, based on UCERF3 Table B1.
39	North Frontal Thrust (W)	0.05-0.2 (0.1)	B	split	R	in UCERF3, N Frontal E and North Frontal W (same rates). USGS: 0.2-1
40	Lenwood	0.6-1.4 (1)	A	split	RL	Model fault is Lenwood plus Lockheart fault to the north USGS rate is 0.2 - 1
41	free-splitting nodes			free-splitting	free	e.g. north end of San Gabriel fault where it meets SAF (complex) Model solves for split direction and rate
42	North Frontal Thrust (E)	0.05-0.2 (0.1)	na	split	R	No Quaternary geological rate available.
43	San Jacincto Fault: Clark and Coyote Creek, Superstition Hills	7-21 (13)	A	split	RL	Sum of the parallel, closely-spaced Clark and Coyote Creek faults

Group	Name	UCERF3 Avg Rate range	UCERF3 Category	Split or slippery	Slip sense	Notes
44	Hollywood-Raymond Fault	0.2-1.5 (0.9) H 1-5(2) R	C (HF), B (RF)	split	LL	Go with the Raymond rate
45	Santa Monica Fault Malibu?	0.5-2 (1)	D	split	LL-R	Malibu: 74° dip
46	N Hosgri	1-5 (2.5)	B	split	RL	same for all Hosgri
47	Big Pine Fault	0.2-1 (0.4)	na	split	LL	Dips 50° to 70° highest rate is for BP E. BP W and BP central rates are < 0.2 mm/y. UCERF3 slip rate bounds based on USGS slip rate category. No geologic Quaternary rates.
48	Ventura-Oak Ridge and related faults: W	2.5-16 (5.6)	D(Ventura) B (Oak Ridge)	split	R	Sum of Oak Ridge and Ventura slip rates. These faults dip 55-65 degrees, opposite direction, to accommodate N-S shortening. Further west: similar rate from summing Ventura, Red Mt and Oak Ridge (offshore) rates. (For shortening, multiply rate by cosine of 60°)
49	Ventura-Oak Ridge and related faults: E (lumping all to grp 48 May 2, 2015 EHH)	3.5-19 (12)	D(Ventura ra F) B (Oak Ridge)	split	R	Sum of Santa Susana and San Cayetano rates. These faults dip 42-55 degrees, opposite direction, to accommodate N-S shortening. (For shortening, multiply rate by cosine of 50°)
50	San Gorgonio Pass SAF	4-16	na	split	RL	No grade for slip rate. UCERF3 rate adopted from UCERF2.
55	Palos Verdes ext to S boundary			split	RL	use same rates as Palos Verdes Fault (group 22)
56	Imperial ext. to S bdry			split	RL	use same rates as Imperial Fault (group 9)

TABLE 2 - Model Suites

	Locked?	Calibrated to	Notes
Suite 1	Y, variable	GPS	boxcar x 2 sav36a
Suite 1A	Y, variable	GPS, corrected	sav37
Suite 1B	Y, variable	GPS, corrected	like 1A but segment 8 and 9 rates fixed sav38
Suite 1C	Y, variable	GPS	like 1 but segment 8, 9 and 56 rates fixed sav39
Suite 1D	N	GPS	sav41: compare with 36a
Suite 2	N	Strain energy minimization	sav32, revised
Suite 2A	Y, variable	Strain energy minimization	sav40

TABLE 3A - GPS-INFERRED SLIP RATES

Seg	Fault segment name	UCERF 3 Range	Expanded range	Suite 1 sav36a	Suite 1A sav37	Suite 1B sav38	Suite 1C sav39	Suite 1D sav41
3	SAF Mojave N	25-40	17.5-47.5	17.5-24.2	17.5-26.3	17.5-26 17.5-30 vis	17.5-22.7 bf 17.5-26 vis	17.7 to 20.9
5	SAF Carrizo	31-37	28-40	28-32	28-34.6	28-31.8	28-30.9	28-34
34	SAF Mojave S	25-40	17.5-47.5	17.5-20.6	17.5-35	17.5-32.9	17.5-22.9	17.7 to 20.6
7	SAF San Bernardino	5-20	0-37.5	-	5.1-29	3.8-29	-	-
8	SAF Coachella	15-30	7.5-37.5	30.4-38.0	28-38 bf	na	na	13.5-38
9	Imperial	15-40	2.5-52.5	38.5-52.5	44-52.5 bf	na	na	25-52.5
50	San Gorgonio Pass SAF	4-16	0-22	2.5-12.5	2.6-11.2	2.5-7.3	2.5-7.3	-
13	San Jacinto N	11-18	7.5-21.5	13.8-21.5	18.1-21.5	13.4-21.5	17.6-21.5 bf 9-21.5 vis	- 10-19 vis
26	San Jacinto central	11-18	7.5-21.5	-	-	-	-	-
43	San Jacinto S	7-21	0-28	-	-	5.5-24.7	0-25	-
48	Ventura-Oak Ridge	2.5-16	** 3 - 8.5?	3.1-7.6	3.1-5.7	3-7.6	3-6	-
10	West Garlock	5-11	2-14	2-14	2.6-14	-	-	-
11	Central Garlock	5-9	3-11	-	5.4-11	-	-	-

12	East Garlock	1-5	0-7	-	0-5.7	-	-	-
20	Elsinore	3-7	1-9	1-8.4	1-3.7	-	- 1-6 vis	1-6.5
21	Newport-Inglewood	0.5-3	0-5	-	-	-	-	-
22	Palos Verdes	2-5	0.5-6.5	0.5-4.4	0.5-5.1	0.5-5	0.5-5.2	0.5-3.5 (0.5-5.5 vis)
24	S San Clemente	1.5-5	0-7	0.2-6	0-5.6	0-5.8	- bf 0-5 vis	0-5.5
14	Death Valley	3-6	1.5-7.5	3.7-7.5	2.6-7.5	-	2.7-7.5	-
15	Fish Lake Valley	2-4	1-5	1.7-5	-	-	-	-
16	Panamint Valley	1-5	0-7	1.3-7	1.7-7	-	-	-
35	Pinto Mountain	1-5	0-7	-	-	-	-	-
38	Landers-Gravel Hill	0.5-2.1	0-3	-	-	- vis 1-3	-	1.8-3 (0.5-3 vis)
40	Lenwood	0.6-1.1	0-1.8	1.4-1.8	-	-	-	-
19	Owens Valley	2-5	0.5-6.5	1.2-6.5	5.4-6.5 bf	-	1.6-6.5	- (1-6.5 vis)
23	N San Clemente	1-5	0-9	0-6.7	-	-	- bf 0-5 vis	-

Within the fault slip rate ranges shown, the WRSS for the best model incorporating each slip rate is within 2% of the value for the best overall model in the suite. To obtain this range, the minimum WRSS values for each slip rate were fit to a quadratic function of slip rate. “vis” and “bf” refer to visible estimates of the slip rate range, or bad fits, because the WRSS values were not well fit by a quadratic function.

TABLE 3B - TSE-INFERRED SLIP RATES: SUITE 2

Seg	Fault segment name	UCERF3 Range	Expanded range	Best and (90% CI range), Suite 2 (sav32) (unlocked)	Suite 2A (sav40) (locked)
3	SAF Mojave N	25-40	17.5-47.5	20.1-36.3	17.5-33 (17.5-30 vis)
5	SAF Carrizo	31-37	28-40	30.5-40 bf	28-33 (- vis)
34	SAF Mojave S	25-40	17.5-47.5	17.5-25.7	17.5-24.5 (17.5-32 vis)
7	SAF San Bernardino	5-20	0-27.5	- bf 0-20 vis	0-20 (0-15 vis)
8	SAF Coachella	15-30	7.5-37.5	7.5-13.8	6-12.5 (6-17 vis)
9	Imperial	15-40	2.5-52.5	17.2-42.2	2.7-18
50	San Gorgonio Pass SAF	4-16	0-22	4-13	-
13	San Jacinto N	11-18	7.5-21.5	7.5-10.7	7.5-12.6
26	San Jacinto central	11-18	7.5-21.5	17-21.2 bf	-
43	San Jacinto S	7-21	0-28	0-21.1 bf 10-25 vis	0-14 (2-11 vis)
48	Ventura-Oak Ridge	2.5-16	** 3 - 8.5?	- bf 4-7 vis	-
10	West Garlock	5-11	2-14	3.5-10.5	-
11	Central Garlock	5-9	3-11	3.1-10 bf	-
12	East Garlock	1-5	0-7	0-5.8	-
20	Elsinore	3-7	1-9	-	- (vis 1-6)

21	Newport-Inglewood	0.5-3	0-5	-	-
22	Palos Verdes	2-5	0.5-6.5	- bf 3-6 vis	- (1-5 vis)
24	S San Clemente	1.5-5	0-7	2.1-6.6	-
14	Death Valley	3-6	1.5-7.5	-	-
15	Fish Lake Valley	2-4	1-5	-	-
16	Panamint Valley	1-5	0-7	-	-
35	Pinto Mountain	1-5	0-7	-	- (2-7 vis)
38	Landers-Gravel Hill	0.5-2.1	0-3	-	
40	Lenwood	0.6-1.1	0-1.8	1-1.8	
19	Owens Valley	2-5	0.5-6.5	0.6-4.7	
23	N San Clemente	1-5	0-9	5.6-6.6 bf 4-6 vis	

Within the fault slip rate ranges shown, the TSE for the best model incorporating each slip rate is within 2% of the value for the best overall model in the suite. To obtain this range, the minimum TSE values for each slip rate were fit to a quadratic function of slip rate. “vis” and “bf” refer to visible estimates of the slip rate range, or bad fits, because the TSE values were not well fit by a quadratic function.